Bell-inequality violation by dynamical Casimir photons in a superconducting microwave circuit

Riddhi Chatterjee [*] and A. S. Majumdar[†]

S. N. Bose National Centre for Basic Sciences, Block JD, Sector III, Salt Lake, Kolkata 700106, India

We study the Bell's inequality violation by dynamical Casimir radiation with pseudospin measurement. We consider a circuit quantum electrodynamical setup where a relativistically moving mirror is simulated by variable external magnetic flux in a superconducting quantum interference device terminating a superconducting-microwave waveguide. We analytically obtain expectation values of the Bell operator optimized with respect to channel orientations in terms of the system parameters. We consider the effects of local noise in the microwave field modes, asymmetry between the field modes resulting from nonzero detuning, and signal loss. Our analysis provides ranges of the above experimental parameters for which the Bell violation can be observed. We show that the Bell violation can be observed in this setup up to 40 mK temperature as well as up to 65% signal loss.

I. INTRODUCTION

A fluctuating vacuum of quantum fields produces particles when the geometry of the background space-time is curved or changes with time. A quantized vacuum emits particles known as Hawking radiation [1] due to gravity in the space-time of black holes. Cosmological particle production can be explained as the radiation by the quantum vacuum in the expanding universe [2–4]. Radiation by the quantized vacuum occurs inside cavities [5] and in free space [6,7] in the presence of moving mirrors or when the field is subjected to time-dependent boundary conditions. This phenomena is called the dynamical Casimir effect (DCE) or Moore-DeWitt effect [5,6].

The physics of these quantum radiations have profound significance in the foundations of quantum theory in curved space-time [3], which predicts that the emitted particles have blackbody distribution [8–10]. Thermodynamics of black holes [9] may give rise to the information paradox, which has been a subject of much debate [11]. This motivated the study of quantum correlations in Hawking radiation [12–14]. Extensive studies were performed on various foundational and informational theoretic aspects in curved space-time [12–21]. However, the experimental detection of such radiation in nature seems to be out of reach of current technology.

With the development of quantum material technology, it has been possible to create analog DCE in the laboratory by varying bulk properties of materials such that time-dependent boundary conditions are induced (quantum simulation of a moving mirror) in the medium containing the quantum field [22–25]. The time-dependent boundary condition makes the vacuum state of the field evolve into a superposition of states of various numbers of particles, as denoted mathematically by a Bogolyubov transformation [7,10,26]. This results in

the emission of Casimir photon pairs. If the background space-time is flat apart from the boundary condition, the emission can be localized as the radiation from a moving mirror [5,7,10,26]. A relativistically moving mirror causes the rapid nonadiabatic modulation of quantum field modes. To accommodate the modulated modes, the quantum vacuum throws up particles that follow Planck's distribution.

Though for the case of the nonrelativistically moving mirror, particles can be created through nonuniform acceleration, the rate of particle production is extremely small [5]. Moreover, a cavity setup is generally introduced to obtain parametric amplification. In practice, making a mechanical mirror move near the speed of light has been technologically challenging for a long time. DCE was first observed experimentally [24,25] in superconducting microwave circuits by simulating the relativistic motion of mirrors [22,23]. Here the superconducting transmission line is interrupted by superconducting quantum interference devices (SQUIDs). Inductance of the SQUID is ultra-rapidly tuned by making high-frequency modulation of the external magnetic flux threading the SQUID. Change in the inductance causes change in the electrical length of the transmission line. Hence, a time-dependent boundary condition similar to that induced by a relativistically moving mirror is imposed to the quantized microwave field in the transmission line through the screening current flowing through the SQUID. In the above circuit quantum electrodynamical (cQED) setup, the simulated velocity of the mirror can reach $\sim 10^6$ m s^{-1}, and the number of photons generated per second is 10^5 [23]. DCE can also be implemented in the optomechanical setup [27].

DCE entangles the field modes and the nature of the radiation is nonclassical [28]. Entanglement in the DCE is a consequence of the energy and momentum conservation, just like in the parametric down-conversion process. Quantum correlations generated through DCE can be used as a resource for quantum information processing. Even in a realistic cQED setup where the background noise is present, the microwave radiation can be nonclassical [28]. Apart from its significance

―――――
*riddhichatterjee27@gmail.com
†archan@bose.res.in

as a resource for quantum tasks, the above experimental setup provides a platform for simulation of fundamental phenomena [20,21,29]. Quantum features such as entanglement, coherence, and discord of noisy Casimir photons were studied with respect to various circuit parameters [30,31]. Gaussian interferometric power and steering were also studied in the presence of noise [32–34].

The Bell nonlocality is the strongest of all quantum correlations, manifesting the violation of local realism [35,36]. Bell presented his seminal work as a quantitative formulation of the ideas of Einstein, Podolsky, and Rosen (EPR) that suggested quantum mechanics as an incomplete theory [37]. EPR based their argument on states having a continuous spectrum in phase space. However, the formalisms of Bohm [38] and Bell [35,36] were based on discrete dimensional systems, as was the work of Clauser, Horne, Shimony, and Holt (CHSH) [39]. Subsequently, Bell's inequality violation has been extensively investigated both in discrete and continuous variable systems [40–48]. The significance of Bell nonlocality in the security of quantum cryptography [49–52] has come under sharper focus with the development of device-independent quantum key distribution protocols [53–55]. Bell's inequality violation was studied in diverse domains ranging from fundamental phenomena such as the Unruh effect [56] and cosmic photons [57,58] to the case of laboratory experiments using quantum materials [59,60].

In this work we investigate Bell's inequality violation by dynamical Casimir radiation using non-Gaussian pseudospin measurements. Our primary motivation arises from the fact that the study of Bell's inequality in the context of particle production through time-dependent boundary conditions was hitherto unexplored in the literature, even though the system of circuit quantum electrodynamics with a moving mirror can be implemented in the laboratory [24,25]. Fundamentally, the dynamical space-time background generally produces Gaussian states. The quantum state of the microwave Casimir photons is a two-mode squeezed thermal state [22–24,28,30–34], though a NOON state was also engineered using the DCE array [61]. Several studies were performed on quantum correlations of Casimir photons based on Gaussian measurement [28,30–34]. Here we explore quantum correlations of DCE radiation with measurement beyond the Gaussian regime. Non-Gaussian measurement is a significant tool in quantum information such as quantum teleportation [62], steering and cryptography [63–65], and non-Gaussian state preparation from a Gaussian state [66]. As it is possible to implement DCE in the laboratory, our analysis should be relevant to understand the efficiency of DCE as a resource for quantum information.

Our approach is based on employing pseudospin mesurements represented in configuration space [46,47]. Such measurements were used to study the Bell nonlocality of a two-mode squeezed vacuum [46,47], cosmic photons [58], and quantum steering of a two-mode squeezed thermal state [64]. The pseudospin operators represented in configuration space are easier to handle compared to their representation in the number basis [64]. It may be noted that optimization of the expectation value of the Bell operator in configuration space involves additional parameters compared to that in the number state representation [46]. Pseudospin measurement in configuration space was also used to study nonlocality of

different classes of multimode Gaussian states [67], the enhancement of nonlocality [68], and quantum teleportation [62]. Our aim is to use this measurement to explore the Bell-CHSH inequality violation by Casimir photon pairs in the cQED setup. We investigate how the optimal value of the Bell violation depends on various circuit parameters. Specifically, we consider the effect of local noise, nonzero detuning, and signal loss.

Our work is organized as follows. In Sec. II we describe DCE in the cQED setup. In Sec. III we study violation of the Bell-CHSH inequality by Casimir photon pairs generated via the cQED setup described in Sec. II. We explore the dependence of optimal Bell violations on different system parameters. In Sec. IV we study the robustness of the Bell violation under signal loss. In Sec. V we present a summary of our main results along with some concluding remarks.

II. DCE IN SUPERCONDUCTING CIRCUIT

A. System specification

We consider the cQED setup described in [22–24,28]. A superconducting coplanar waveguide (CPW) with characteristic capacitance C_0 and inductance L_0 per unit length is terminated to ground (say at $x = 0$) by a SQUID loop threaded by external magnetic flux $\phi_{\text{ext}}(t)$. The quantized microwave field inside the waveguide is described by its flux field $\phi^i(x, t)$ that obeys the one-dimensional (1-D) massless Klein-Gordon equation

$$(\partial_{xx} - v^{-2}\partial_{tt})\phi^i(x, t) = 0, \tag{1}$$

with Dirichlet boundary condition at $x = 0$. In the framework of input-output theory, the total flux field in the CPW transmission line is

$$\phi(x, t) = \phi^{\text{in}}(x, t) + \phi^{\text{out}}(x, t), \tag{2}$$

where $\phi^{\text{in}}(x, t)$ and $\phi^{\text{out}}(x, t)$ are the incoming (right moving) and outgoing (left moving) components of the total flux field.

In terms of the second quantized solution of the Klein-Gordon equations, the expression (2) can be written as [22,23,28,69]

$$\phi(x, t) = \sqrt{\frac{\hbar Z_0}{4\pi}} \int_{-\infty}^{\infty} \frac{d\omega}{\sqrt{|\omega|}} \Big[\hat{a}_\omega^{in} \, e^{-i(\omega t - k_\omega x)} + \hat{a}_\omega^{\text{out}} \, e^{-i(\omega t + k_\omega x)} \Big], \quad (x < 0). \tag{3}$$

$\hat{a}_\omega^{\text{in}}$ and $\hat{a}_\omega^{\text{out}}$ are annihilation operators for modes of frequency ω, propagating with velocity v to the right (incoming) and left (outgoing), respectively. $[\hat{a}_\omega^{\text{in(out)}}, (\hat{a}_{\omega'}^{\text{in(out)}})^\dagger] = \delta(\omega - \omega')$ and we use the convention $\hat{a}_{-\omega} = \hat{a}_\omega^\dagger$. The velocity $v = \omega/k_\omega = 1/\sqrt{C_0 L_0}$ and $Z_0 = \sqrt{L_0/C_0}$ is the characteristic impedance of CPW.

At large plasma frequency, when the charging energy is much smaller than the external flux-dependent effective Josephson energy $E_J(t) = E_J[\phi_{\text{ext}}(t)]$, the SQUID is a passive element that provides the following boundary condition at $x = 0$ to the flux field inside CPW line [22,23]

$$\phi(0, t) + L_{\text{eff}}(t) \, \partial_x \phi(x, t)\big|_{x=0} = 0, \tag{4}$$

where $L_{\text{eff}}(t) = L_J(t)/L_0$ and $L_J = (\frac{\phi_0}{2\pi})^2 \frac{1}{E_J(t)}$ is the tunable Josephson inductance of the SQUID. $\phi_0 = (h/2e)$ is the magnetic flux quantum. The boundary condition at $x = 0$ depends only upon the tunable Josephson inductance of the SQUID [22–24], which creates a mirror at an effective length $L_{\text{eff}}(t)$ from the physical end of the CPW line. For sinusoidal modulation $E_J(t) = E_J^0(1 + \epsilon \sin \omega_d t)$ with driving amplitude ϵ and driving frequency ω_d [22,23], the effective length modulation amplitude is $\delta L_{\text{eff}} = \epsilon L_{\text{eff}}^0$, where $L_{\text{eff}}^0 = L_{\text{eff}}(0)$. So, the effective velocity of the mirror is $v_{\text{eff}} = \omega_d L_{\text{eff}}^0$. When v_{eff} is a significant fraction of the velocity v of light in a CPW line, nonadiabatic modulation occurs in the field modes resulting in a significant amount of photon pair production.

In the case of weak harmonic drive (perturbative regime) [22,23], $\epsilon E_J^0 \ll E_J^0$ and the output photon-flux density has a parabolic spectrum with a maximum at $\omega_d/2$. Output photon pairs are correlated with frequency $\omega_{\pm}$, where $\omega_+ + \omega_- = \omega_d$. The simplest choice is $\omega_{\pm} = \omega_d/2 \pm \delta\omega$, where $\delta\omega$ is the detuning parameter. Using Eqs. (3) and (4) and applying scattering theory, the Bogolyubov transformation between incoming and outgoing modes can be obtained analytically in the perturbative regime [23,28,70]

$$\hat{a}_{\omega_{\pm}}^{\text{out}} = -\hat{a}_{\omega_{\pm}}^{\text{in}} - if(\hat{a}_{\omega_{\mp}}^{\text{in}})^{\dagger}, \tag{5}$$

where

$$f = \frac{\epsilon L_{\text{eff}}^0 \sqrt{\omega_+ \omega_-}}{v}. \tag{6}$$

Pair production results in two-mode squeezing of the output field [23,28]. So, if the input state ϕ^{in} in Eq. (2) is a vacuum state, the output DCE state ϕ^{out} is ideally a two-mode squeezed vacuum.

B. Covariance matrix of input or output modes

Let us consider the DCE input or output states in the framework of Gaussian covariance matrix formalism [28]. In our work we follow the convention of [71]. The input or output state can be written in terms of the covariance matrix (CM)

$$V_{\alpha\beta} = \langle \hat{R}_\alpha \hat{R}_\beta + \hat{R}_\beta \hat{R}_\alpha \rangle - 2\langle \hat{R}_\alpha \rangle \langle \hat{R}_\beta \rangle, \tag{7}$$

where $\hat{R} = (\hat{q}_-, \hat{p}_-, \hat{q}_+, \hat{p}_+)^T$ is a vector containing field quadrature elements with $[\hat{q}_\alpha, \hat{p}_\beta] = i\delta_{\alpha\beta}$ and

$$\begin{aligned}
\hat{q}_{\pm}^{\text{in(out)}} &= \frac{\hat{a}_{\omega_{\pm}}^{\text{in(out)}} + (\hat{a}_{\omega_{\pm}}^{\text{in(out)}})^{\dagger}}{\sqrt{2}} \\
\hat{p}_{\pm}^{\text{in(out)}} &= -i \frac{\hat{a}_{\omega_{\pm}}^{\text{in(out)}} - (\hat{a}_{\omega_{\pm}}^{\text{in(out)}})^{\dagger}}{\sqrt{2}},
\end{aligned} \tag{8}$$

where we restricted ourself to a pair of entangled modes $\{\pm\}$ with frequencies adding up to the driving frequency. The nonclassicality of DCE radiation originates from the entanglement of Casimir photon pairs [28]. The ideal input state will be a vacuum state which is impossible to create in practical situations. So, we will use a quasi-vacuum state, containing a small number of thermal photons $\{n_{\pm}^{\text{th}} = (e^{\frac{\hbar\omega_{\pm}}{kT}} - 1)^{-1}\}$ [28,31], as the input state.

Note that the choice of the initial thermal state modifies the Green's function and the power spectrum and the frequencies

of the incoming and outgoing signals are doppler shifted [72]. However, the effect on the correlation of the outgoing modes is negligible for our chosen temperature range [25]. Hence, correlation of the output modes are observed in experiments despite the fact that the effects of temperature are not explicitly monitored during the experiments [25,72]. The quadrature elements have zero first-moment. The CM of the input field is given by

$$V_{\text{in}} = \begin{pmatrix} n_0 & 0 & 0 & 0 \\ 0 & n_0 & 0 & 0 \\ 0 & 0 & m_0 & 0 \\ 0 & 0 & 0 & m_0 \end{pmatrix} \tag{9}$$

where

$$\begin{aligned}
n_0 &= (2n_-^{\text{th}} + 1), \\
m_0 &= (2n_+^{\text{th}} + 1).
\end{aligned} \tag{10}$$

Using Eqs. (5), (6), (8), (9), and (10), the CM of the output field is obtained (in standard form) as

$$V_{\text{out}} = \begin{pmatrix} n & 0 & r & 0 \\ 0 & n & 0 & -r \\ r & 0 & m & 0 \\ 0 & -r & 0 & m \end{pmatrix}, \tag{11}$$

where

$$\begin{aligned}
n &= (2n_-^{\text{th}} + 1) + f^2(2n_+^{\text{th}} + 1), \\
m &= (2n_+^{\text{th}} + 1) + f^2(2n_-^{\text{th}} + 1), \\
r &= 2f(n_+^{\text{th}} + n_-^{\text{th}} + 1).
\end{aligned} \tag{12}$$

V_{out} corresponds to a two-mode squeezed thermal state with squeezing parameter $2f$.

III. BELL VIOLATION BY DCE RADIATION

We study Bell's inequality violation by the output DCE radiation described by the CM in Eqs. (11) and (12), using the definition of the pseudospin measurement represented in configuration space [46,47]

$$\begin{aligned}
\hat{\Pi}_x &= \int_0^\infty dq[|\mathcal{Q}^+\rangle \langle \mathcal{Q}^-| + |\mathcal{Q}^-\rangle \langle \mathcal{Q}^+|], \\
\hat{\Pi}_y &= i \int_0^\infty dq[|\mathcal{Q}^+\rangle \langle \mathcal{Q}^-| - |\mathcal{Q}^-\rangle \langle \mathcal{Q}^+|], \\
\hat{\Pi}_z &= -\int_0^\infty dq[|\mathcal{Q}^+\rangle \langle \mathcal{Q}^+| - |\mathcal{Q}^-\rangle \langle \mathcal{Q}^-|],
\end{aligned} \tag{13}$$

where the channels $|\mathcal{Q}^+\rangle$ and $|\mathcal{Q}^-\rangle$ are given by

$$\begin{aligned}
|\mathcal{Q}^+\rangle &= \frac{1}{2}[|q\rangle + |-q\rangle], \\
|\mathcal{Q}^-\rangle &= \frac{1}{2}[|q\rangle - |-q\rangle].
\end{aligned} \tag{14}$$

$\{\hat{\Pi}_x, \hat{\Pi}_y, \hat{\Pi}_z\}$ satisfy $SU(2)$ algebra. Following [46], the Bell operator is defined as

$$\begin{aligned}
\mathcal{B} = &\vec{a} \cdot \hat{\Pi}^{(-)} \otimes \vec{b} \cdot \hat{\Pi}^{(+)} + \vec{a} \cdot \hat{\Pi}^{(-)} \otimes \vec{b}' \cdot \hat{\Pi}^{(+)} \\
&+ \vec{a}' \cdot \hat{\Pi}^{(-)} \otimes \vec{b} \cdot \hat{\Pi}^{(+)} - \vec{a}' \cdot \hat{\Pi}^{(-)} \otimes \vec{b}' \cdot \hat{\Pi}^{(+)},
\end{aligned} \tag{15}$$

where $\vec{a}, \vec{a}', \vec{b}, \vec{b}'$ are the unit vectors that specify the orientation of the first and second channels, respectively. $\hat{\Pi}^{(\pm)}$ designates channel $\hat{\Pi}$ applied on the $\{\pm\}$ mode.

To calculate the optimal Bell violation, first we perform orientational optimization of the measurement directions following [45,46,48]. We choose $\vec{a}, \vec{a}', \vec{b}, \vec{b}'$ in the spherical polar coordinate as

$$\phi_a = \phi_{a'} = \phi_b = \phi_{b'} = 0,$$
$$\theta_a = 0, \quad \theta_{a'} = \pi/2, \quad \theta_b = -\theta_{b'}. \tag{16}$$

So, the Bell operator reduces to

$$\mathcal{B} = 2\left(\cos\theta_b \, \hat{\Pi}_x^{(-)} \otimes \hat{\Pi}_x^{(+)} + \sin\theta_b \, \hat{\Pi}_z^{(-)} \otimes \hat{\Pi}_z^{(+)}\right). \tag{17}$$

Maximizing over θ_b we get the maximal expectation value of $\mathcal{B}$,

$$B_{\max} = 2\sqrt{\left\langle\hat{\Pi}_x^{(-)} \otimes \hat{\Pi}_x^{(+)}\right\rangle^2 + \left\langle\hat{\Pi}_z^{(-)} \otimes \hat{\Pi}_z^{(+)}\right\rangle^2}, \tag{18}$$

where $\langle \cdot \rangle$ is the expectation value of an operator for a given state. Bell violation occurs when

$$B_{\max} > 2. \tag{19}$$

We now calculate $B_{\max}$ for our output state described by the covariance matrix V_{out} in Eqs. (11) and (12) and study how the value of $B_{\max}$ depends upon various system parameters. To calculate the expectation value of two-mode pseudospin operators we use the definitions [47,64]

$$\left\langle\hat{\Pi}_i^{(-)} \otimes \hat{\Pi}_j^{(+)}\right\rangle = \frac{1}{(2\pi)^2} \int d^4X \, W_{\mathrm{out}}(X)$$
$$\times \, W_{\hat{\Pi}_i^{(-)}}(q_-, p_-) \, W_{\hat{\Pi}_j^{(+)}}(q_+, p_+), \tag{20}$$

where $X = (q_-, p_-, q_+, p_+)^T$,

$$W_{\hat{\Pi}_x}(q, p) = \mathrm{sgn}(q),$$
$$W_{\hat{\Pi}_z}(q, p) = -\pi\delta(q)\delta(p), \tag{21}$$

and the Wigner function of the output state is

$$W_{\mathrm{out}}(X) = \frac{1}{\pi^2} \frac{1}{\det(V_{\mathrm{out}})} e^{-(X^T \, V_{\mathrm{out}}^{-1} \, X)}. \tag{22}$$

Plugging everything in Eq. (18) we evaluate $B_{\max}$ for output DCE radiation in terms of circuit parameters

$$B_{\max} = 2\left(\frac{1}{(f^2-1)^4(2n_-+1)^2(2n_++1)^2}\right.$$
$$\left. + \frac{4\tan^{-1}\left(\frac{4f^2(n_-+n_++1)^2}{(f^2-1)^2(2n_-+1)(2n_++1)}\right)^2}{\pi^2}\right)^{1/2}, \tag{23}$$

with $\{n_\pm\}$ defined above in Eq. (9) and f is given by Eq. (6), as a function of driving amplitude ϵ. Now we plot the variation of $B_{\max}$ with respect to different experimental parameters to observe the Bell's inequality violation.

Figure 1 shows the variation of $B_{\max}$ with increasing driving amplitude ϵ in different temperatures of the system. Here detuning is zero, which means $n_- = n_+$ and hence both modes are symmetric and have equal local noises. The driving amplitude is considered up to $\epsilon = 0.6$, which corresponds to $f = 0.0786$ which is well inside the perturbative regime. The
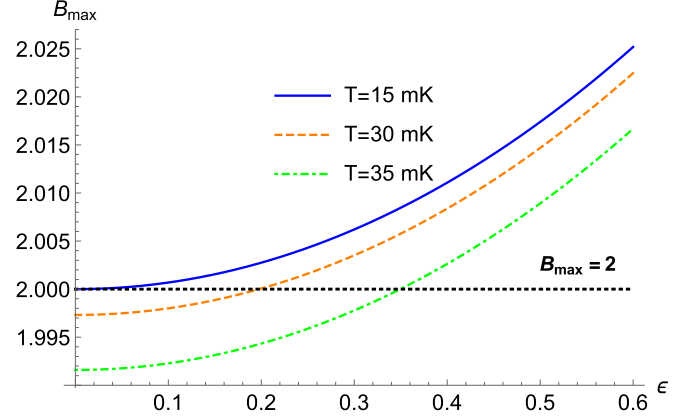

FIG. 1. Variation of $B_{\max}$ with the driving amplitude ϵ in different temperatures of the system. Driving frequency $\omega_d = 20\pi$ GHz. $v = 1.2 \times 10^8$ ms^{-1}. $L_{\mathrm{eff}}^0 = 0.5$ mm. Detuning $\delta\omega = 0$.

plot shows that the value of $B_{\max}$ has dropped significantly at $T = 35$ mK compared to its values at $T = 15$ mK and 30 mK. Also at 35 mK, it requires significantly larger driving amplitude >0.35 to observe Bell's inequality violation compared to the other two temperatures. The highest value of the Bell violation obtained here, at 15 mK and with $\epsilon = 0.6$, is 2.025.

Figure 2 shows the variation of $B_{\max}$ with the increase in driving amplitude ϵ and $\frac{\delta\omega}{\omega_d}$ which is detuning expressed as a fraction of driving frequency ω_d. The dash-dotted curve represents the points $B_{\max} = 2$. So, the region on the right side of this curve violates Bell's inequality. The increase in detuning increases the asymmetry between the two modes, decreasing the value of $B_{\max}$. The plot also shows that, to observe Bell's inequality violation in the chosen parameter range, detuning needs to satisfy $\frac{\delta\omega}{\omega_d} < 0.27$.

Figure 3 shows the variation of $B_{\max}$ with the increase in temperature T and $\frac{\delta\omega}{\omega_d}$ which is detuning expressed as a fraction of driving frequency ω_d. The dash-dotted curve represents
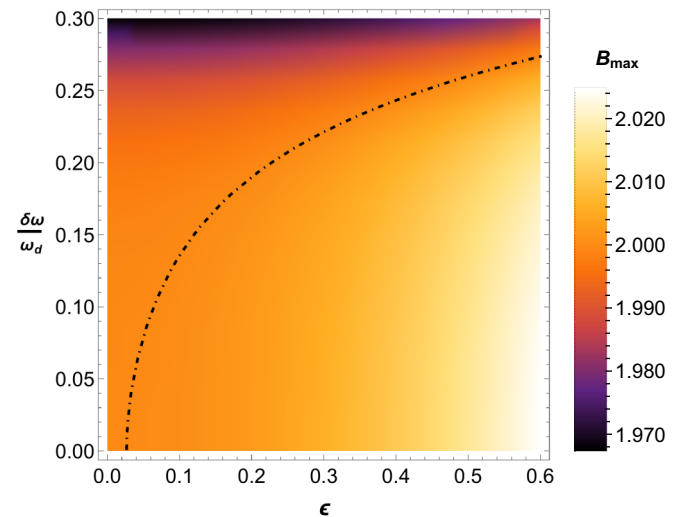

FIG. 2. Variation of $B_{\max}$ with respect to the driving amplitude ϵ and detuning $\delta\omega$ as the fraction of driving frequency $\omega_d = 20\pi$ GHz. $v = 1.2 \times 10^8$ ms^{-1}. $L_{\mathrm{eff}}^0 = 0.5$ mm. $T = 20$ mK.
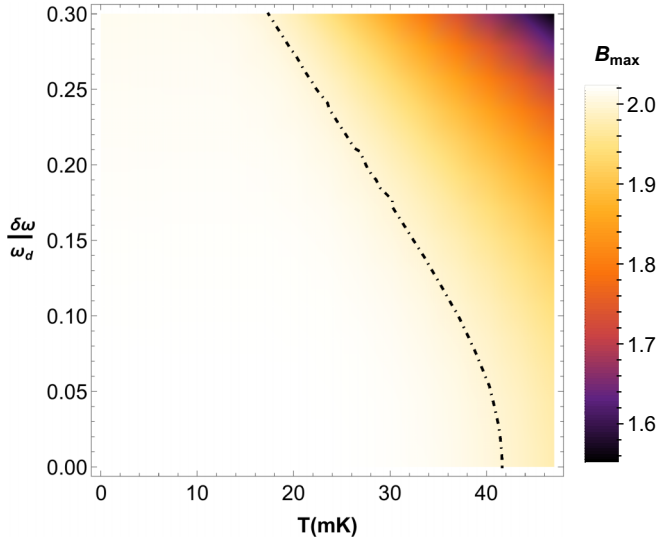
FIG. 3. Variation of $B_{\max}$ with respect to the temperature T (mK) and detuning $\delta\omega$ as the fraction of driving frequency $\omega_d = 20\pi$ GHz, with $v = 1.2 \times 10^8$ ms^{-1}, $L_{\text{eff}}^0 = 0.5$ mm, and $\epsilon = 0.6$.

the points $B_{\max} = 2$. The region on the left side of this curve violates Bell's inequality. The plot indicates that at very low temperature, the effect of detuning on the value of $B_{\max}$ is not significant and Bell violation is always achieved. This is because at low temperature, local noise is very small and hence the asymmetry between the modes is very small even with a significant value of detuning and driving amplitude ϵ [driving parameter f is a function of detuning and driving amplitude, see Eq. (6)]. For temperature 20–30 mK, the value of $B_{\max}$ falls below 2 for significant detuning. Around temperature 34 mK, Bell violation is absent when $\frac{\delta\omega}{\omega_d}$ is approximately greater than 0.15. For temperature $T \geqslant 42$ mK, Bell's inequality violation is completely absent for our chosen parameter range.

IV. ROBUSTNESS UNDER SIGNAL LOSS

In realistic scenarios, an experiment may suffer from imperfections. The two most relevant types of noise in the present setup are noise due to the presence of thermal photons in the signal and signal loss in the transmission line. In our analysis we considered both the above types of noise. The thermal noise that is observed to be present in DCE experiments implemented so far [24,25,73] is taken into account in our analysis. We further study the tolerance of nonlocality of DCE radiation under another source of experimental defect, *viz.*, photon loss which is, in general, one of the most studied defects in the context of Bell violation [74]. Signal loss can occur due to various reasons such as the presence of impurities, measurement inefficiency, and so on [75], and has been discussed in the context of generation and measurement of DCE radiation [24,25,73]. In our study we mimic the signal loss by beam splitter operation and study the tolerance of Bell nonlocality of DCE radiation against such noise.

Our goal here is to study if we can observe Bell's inequality violation in the experimental setup under consideration in the presence of signal loss in one of the modes (say the first

mode). We apply a pure loss channel on mode $\{-\}$ and obtain the output covariance matrix following the method of the authors of [64]. We couple the state described by V_{out}, with a single-mode vacuum (ancilla). Thus, the resultant covariance matrix is given by $V' = V_{\text{anc}} \oplus V_{\text{out}}$, where $V_{\text{anc}} = \mathbb{1}_{2 \times 2}$ is the covariance matrix of the ancilla, with $\mathbb{1}_{2 \times 2}$ being the 2×2 identity matix. We next transform the ancillary mode and $\{-\}$ mode though the beam splitter channel B_s. We apply $B_s \oplus \mathbb{1}_{2 \times 2}$ on V' where

$$B_s = \begin{pmatrix} \sqrt{\eta} \, \mathbb{1}_{2 \times 2} & -\sqrt{1-\eta} \, \mathbb{1}_{2 \times 2} \\ \sqrt{1-\eta} \, \mathbb{1}_{2 \times 2} & \sqrt{\eta} \, \mathbb{1}_{2 \times 2} \end{pmatrix}, \qquad (24)$$

with $\eta \in (0, 1)$ being the transmission efficiency. Tracing out the ancillary modes leads us to obtain the covariance matrix of the output DCE radiation with signal loss on mode $\{-\}$, given by

$$V_{\text{out}}^L = \begin{pmatrix} n' & 0 & r' & 0 \\ 0 & n' & 0 & -r' \\ r' & 0 & m' & 0 \\ 0 & -r' & 0 & m' \end{pmatrix}, \qquad (25)$$

where

$$\begin{aligned} n' &= \eta[f^2(2n_+ + 1) + 2n_- + 1] - \eta + 1, \\ m' &= (2n_+^{th} + 1) + f^2(2n_-^{th} + 1), \qquad (26) \\ r' &= 2f\sqrt{\eta}(n_- + n_+ + 1), \end{aligned}$$

and $\{n_\pm\}$, f have the same definitions as in Eq. (12). Following a similar procedure as in Sec. III, we find the expectation value of the Bell operator, optimized with respect to the measurement orientations for the state described by the covariance matrix V_{out}^L in terms of the system parameters in the presence of signal loss, given by

$$B_{\max}^L = 2\sqrt{\frac{4}{\pi^2} \tan^{-1} (A_1/A_2)^2 + 1/(A_2)^2}, \qquad (27)$$

where

$$\begin{aligned} A_1 &= 4f^2\eta(n_- + n_+ + 1)^2, \\ A_2 &= -4f^2\eta(n_- + n_+ + 1)^2 \\ &\quad + [(2f^2n_- + f^2 + 2n_+ + 1) \qquad (28) \\ &\quad \times (f^2\eta + 2f^2\eta n_+ + 2\eta n_- + 1)]. \end{aligned}$$

We plot the variation of $B_{\max}^L$ with respect to various system parameters to observe the violation of Bell's inequality under signal loss.

Figure 4 shows the variation $B_{\max}^L$ with respect to the driving amplitude ϵ and transmission efficiency η in the absence of detuning. The dash-dotted curve represents the points $B_{\max} = 2$. The region above this curve violates Bell's inequality. Below $\eta = 0.4$, the threshold of Bell violation becomes less sensitive to the increase of the driving amplitude. Bell violation is completely absent when $\eta < 0.35$, i.e., when the signal loss is greater than 65%. The plot indicates that to observe noticeable Bell violation for our chosen range of parameters, the transmission efficiency should be greater than 0.4.
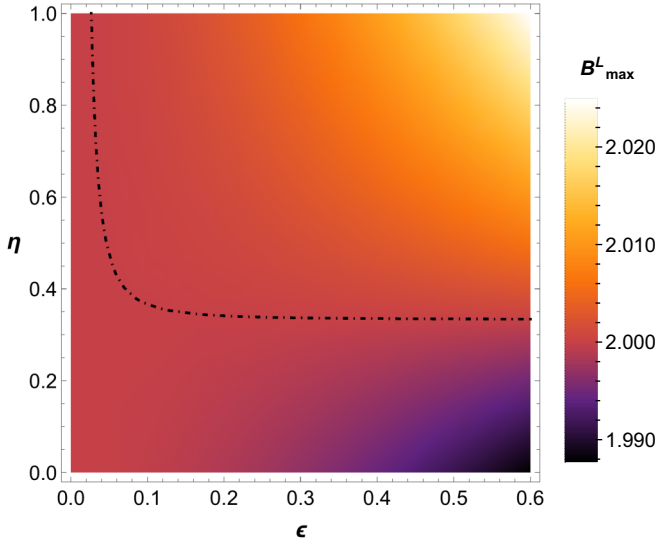
FIG. 4. Variation of $B_{\max}^L$ with respect to the driving amplitude ϵ and transmission efficiencies η. Driving frequency $\omega_d = 20\pi$ GHz. Detuning $\delta\omega = 0$. $v = 1.2 \times 10^8$ ms^{-1}. $L_{\mathrm{eff}}^0 = 0.5$ mm. $T = 20$ mK.

FIG. 6. Variation of $B_{\max}^L$ with respect to the transmission efficiency η and the detuning as a fraction of the driving frequency $\omega_d = 20\pi$ GHz. $v = 1.2 \times 10^8$ ms^{-1}. $L_{\mathrm{eff}}^0 = 0.5$ mm. $\epsilon = 0.6$, $T = 20$ mK.

Figure 5 shows the variation $B_{\max}^L$ with respect to the temperature T and transmission efficiency η in the absence of detuning. The dash-dotted curve represents the points $B_{\max} = 2$. The region above this curve violates Bell's inequality. For temperature above 24 mK, Bell violation is absent when the transmission efficiency $\eta < 0.35$ (signal loss >65%). For higher temperatures, a greater amount of transmission efficiency is needed to observe Bell violation. At temperatures near 40 mK, the transmission efficiency has to be greater than 0.8 (signal loss is required to be less than 20%) for our chosen range of parameters.

Figure 6 shows the variation of $B_{\max}^L$ with respect to the transmission efficiency η and the detuning as a fraction
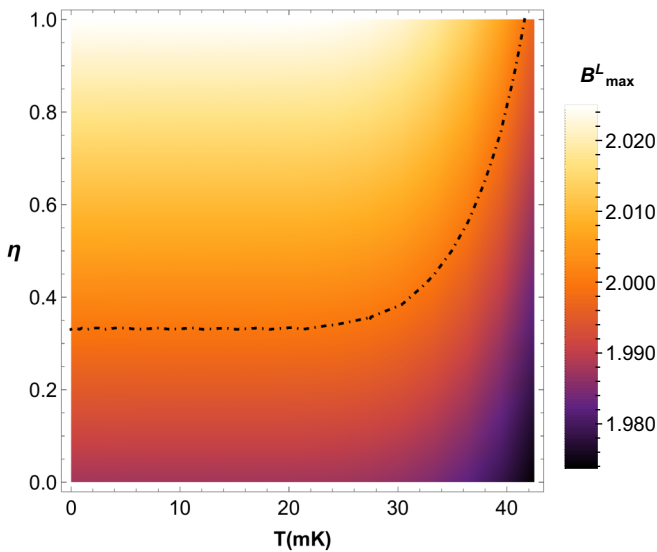
of the driving frequency ω_d. The dash-dotted curve represents the points $B_{\max} = 2$. The region above this curve violates Bell's inequality. The plot indicates that Bell violation occurs for $\eta \geqslant 0.35$ (signal loss $\leqslant 65\%$) up to the detuning $\frac{\delta\omega}{\omega_d} = 0.2$. However, for the value of detuning $0.2 < \frac{\delta\omega}{\omega_d} < 0.27$, a higher transmission efficiency is required. For detuning $\frac{\delta\omega}{\omega_d} > 0.27$ Bell violation is completely absent irrespective of the value of the transmission efficiency. This is consistent with the result of Fig. 2.

FIG. 5. Variation of $B_{\max}^L$ with respect to the temperature T and transmission efficiency η. Driving frequency $\omega_d = 20\pi$ GHz. Detuning $\delta\omega = 0$. $v = 1.2 \times 10^8$ ms^{-1}. $L_{\mathrm{eff}}^0 = 0.5$ mm. $\epsilon = 0.6$.
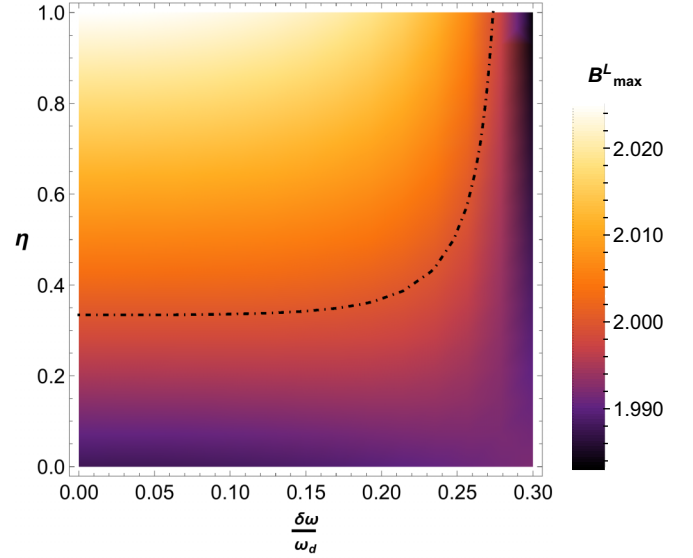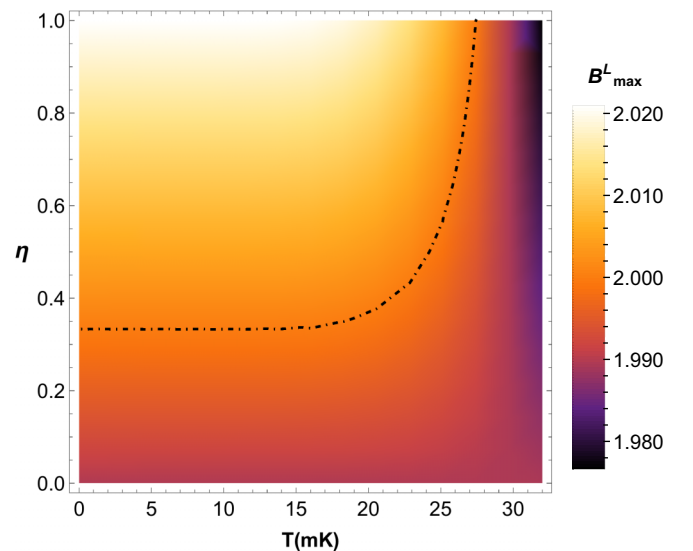

FIG. 7. Variation of $B_{\max}^L$ with respect to the temperature T and transmission efficiency η. $(\delta\omega/\omega_d) = 0.2$ where $\delta\omega$ is the detuning and $\omega_d = 20\pi$ GHz is the driving frequency. $v = 1.2 \times 10^8$ ms^{-1}. $L_{\mathrm{eff}}^0 = 0.5$ mm. $\epsilon = 0.6$.

Figure 7 shows the variation of $B_{\max}^L$ with respect to the temperature T and the transmission efficiency η in the presence of detuning $\frac{\delta\omega}{\omega_d} = 0.2$. The dash-dotted curve represents the points $B_{\max} = 2$. The region above this curve violates Bell's inequality. From the plot we see that for temperature up to 19 mK Bell violation is absent when the transmission efficiency $\eta < 0.35$ ($>65\%$ signal loss). For temperature higher than 19 mK a greater value of transmission efficiency is required to observe Bell violation. $B_{\max}^L$ falls sharply with increasing signal loss for temperature $T > 21$ mK. For our chosen range of parameters Bell violation is absent when $T \geqslant 28$ mK.

Though the main purpose of the present work is to show that Bell violation is indeed possible in the DCE setup, it is also indeed feasible to conceive schemes to experimentally measure such Bell violation. Entanglement in DCE radiation was quantitatively measured in a recent experiment in a superconducting circuit [73]. Experimental studies on DCE radiation show that, in our chosen temperature range, the thermal photons are quite challenging to resolve. Nonetheless, quantum correlation is observed for some chosen range of parameters in the presence of noise due to thermal photons. Note that Bell-violating states form a subset of all entangled states [76]. Hence, a study of entanglement is not equivalent to a study of Bell violation. In the context of the present setup, the range of system parameters for which Bell violation is obtained is much smaller than that of entanglement.

In the present analysis the Bell operator consists of two measurements $\hat{\Pi}_x \otimes \hat{\Pi}_x$ and $\hat{\Pi}_z \otimes \hat{\Pi}_z$. The measurement $\hat{\Pi}_x$ can be written as $\mathrm{sgn}(\hat{q})$ ($\hat{q} \rightarrow$ canonical position operator) [47]. It is basically the sign of the quadrature and can be measured by the homodyne measurement that was implemented in experiments [24,25]. The operator $\hat{\Pi}_z$ is the parity operator in the spatial basis and it has the same expectation value with the parity operator in the number basis [46]. So, it is possible to measure $\langle \hat{\Pi}_z \otimes \hat{\Pi}_z \rangle$ using a number-resolving detector. Alternatively, parity can also be measured in the spatial basis using a parity analyzer, which is the parity-sensitive Mach-Zehnder interferometer [77,78]. Schemes for implementing the Mach-Zehnder interferometer in the superconducting coplaner waveguide (CPW) were proposed [75]. Detailed discussions on implementing various components such as mirrors, phase shifts, and photon detectors for coincidence circuits in CPW were provided (sse, for instance, [79].

Before concluding, it may be pertinent to note the following issue. There are several important loopholes in the experimental violation of a Bell inequality [80]. Two of the most widely discussed loopholes are the locality loophole and the detection loophole. While the locality loophole cannot be closed in the present setup, further analysis is required in respect to the detection of the loophole here. In general, sufficiently high detector efficiencies enable the closure of the detection loophole in Bell tests involving parametric down conversion [81]. Note that, though in the case of the setup involving DCE photons that we considered here, a small magnitude of Bell violation is obtained in the perturbative regime of the driving amplitude; such violation still persists under considerable signal loss. Moreover, our study indicates

that Bell violation increases with the driving amplitude, and hence, a detailed study will be required involving a nonperturbative analysis in conjunction with tolerance to signal loss to estimate the threshold of detector efficiency needed for the closure of the detection loophole.

V. CONCLUSION

Quantum nonlocality as manifested by the violation of Bell's inequality represents a basic paradigm of quantum theory, which is of importance for the test of foundational principles, as well as for potential technological applications, such as in quantum cryptography. In this work we studied Bell violation by dynamical Casimir photon pairs generated from a quantized vacuum by the relativistic motion of a mirror. We considered the circuit quantum electrodynamical setup that was experimentally implemented [24]. Though Bell's inequality was studied earlier theoretically in the noninertial relativistic domain [56–58], experimental verification of such proposals remain beyond the reach of current technology. However, the framework of Bell violation proposed in the present work can be probed efficiently in the laboratory [22–25].

The analysis performed in this work is based on the measurement-induced spin-like quantum correlations within Casimir photon pairs. Previously, several theoretical and experimental studies were performed on Gaussian quantum correlation of DCE photons using homodyne measurement. Our present study focuses on nonlocal quantum correlations between Casimir photon pairs generated through non-Gaussian measurements [46,47]. Such correlations were shown to be of significance in several domains of quantum information and communication [62–66]. The Bell violation obtained here through the above framework is thus of direct relevance to several information theoretic protocols.

Let us now briefly summarize the main results of our study. We analytically derived the expectation value of the Bell operator for DCE radiation, optimized with respect to channel orientations in the context of pseudospin measurements. We studied the behavior of Bell violation in terms of experimental parameters such as the driving frequency. We further considered the effect of local thermal noise in each mode and asymmetry between the entangled modes introduced through the detuning in the frequency of photon pairs. We show that, for our chosen parameter range, the violation of Bell's inequality can be observed up to the temperature about 40 mK. Our results further show that the asymmetry between the entangled modes degrades the Bell nonlocality at relatively higher temperature. However, at low temperatures detuning has a negligible effect on Bell's inequality violation. Finally, we also derived the expectation value of the Bell operator in the presence of signal loss and explored the robustness of Bell nonlocality in this scenario. We show that, in the system under consideration, Bell nonlocality is robust up to 65% signal loss.

To conclude, in our analysis we presented multiple plots showing the variation of Bell's nonlocality with different circuit parameters in the presence of local noise, asymmetry between the entangled modes because of nonzero detuning, and signal loss. Our results clearly demarcate the parameter

regions where Bell nonlocality of Casimir photons can be observed. The choice of parameters considered in the present study is well within the perturbative regime. Since Bell violation is seen to rise rapidly with the increase of the driving frequency, it is expected that higher values of the driving parameter would yield significantly larger magnitudes of Bell violation. Our results thus motivate further analysis in the nonperturbative framework. It might be also interesting to consider in future works the Bell violation in the cQED setup using other measurement schemes. A comparative analysis of

such studies may lead to an optimal framework for quantum state preparation of Casimir photons as a vital step towards information processing through the cQED setup.

ACKNOWLEDGMENT

[1] S. W. Hawking, Commun. Math. Phys. **43**, 199 (1975).

[2] L. Parker, Phys. Rev. **183**, 1057 (1969); Phys. Rev. D **3**, 346 (1971).

[3] N. Birrell and P. Davies, *Quantum Fields in Curved Space*, Cambridge Monographs on Mathematical Physics (Cambridge University Press, Cambridge, England, 1982).

[4] L. H. Ford, Rep. Prog. Phys. **84**, 116901 (2021).

[5] G. T. Moore, J. Math. Phys. **11**, 2679 (1970).

[6] B. S. DeWitt, Phys. Rep. **19**, 295 (1975).

[7] S. A. Fulling and P. C. W. Davies, Proc. R. Soc. London A **348**, 393 (1976).

[8] L. Parker, Nature (London) **261**, 20 (1976).

[9] S. Carlip, Int. J. Mod. Phys. D **23**, 1430023 (2014).

[10] P. C. W. Davies and S. A. Fulling, Proc. R. Soc. London A **356**, 237 (1977).

[11] W. G. Unruh and R. M. Wald, Rep. Prog. Phys. **80**, 092002 (2017).

[12] J. Maldacena, Nat. Rev. Phys. **2**, 123 (2020).

[13] R. Mahajan, Reson. **26**, 33 (2021).

[14] S. Raju, arXiv:2012.05770.

[15] I. Fuentes-Schuller and R. B. Mann, Phys. Rev. Lett. **95**, 120404 (2005).

[16] N. Liu, J. Goold, I. Fuentes, V. Vedral, K. Modi, and D. E. Bruschi, Classical Quantum Gravity **33**, 175014 (2016).

[17] L. C. Céleri, F. Pascoal, and M. H. Y. Moussa, Classical Quantum Gravity **26**, 105014 (2009).

[18] M. P. E. Lock and I. Fuentes, New J. Phys. **19**, 073005 (2017).

[19] M. O. Scully, S. Fulling, D. Lee, D. Page, W. Schleich, and A. A. Svidzinsky, Proc. Natl. Acad. Sci. USA **115**, 8131 (2018).

[20] A. A. Svidzinsky, J. S. Ben-Benjamin, S. A. Fulling, and D. N. Page, Phys. Rev. Lett. **121**, 071301 (2018).

[21] R. Chatterjee, S. Gangopadhyay, and A. S. Majumdar, Phys. Rev. D **104**, 124001 (2021).

[22] J. R. Johansson, G. Johansson, C. M. Wilson, and F. Nori, Phys. Rev. Lett. **103**, 147003 (2009).

[23] J. R. Johansson, G. Johansson, C. M. Wilson, and F. Nori, Phys. Rev. A **82**, 052509 (2010).

[24] C. M. Wilson, G. Johansson, A. Pourkabirian, M. Simoen, J. R. Johansson, T. Duty, F. Nori, and P. Delsing, Nature (London) **479**, 376 (2011).

[25] P. Lähteenmäki, G. S. Paraoanu, J. Hassel, and P. J. Hakonen, Proc. Natl. Acad. Sci. USA **110**, 4234 (2013).

[26] S. A. Fulling and G. E. A. Matsas, Scholarpedia **9**, 31789 (2014).

[27] V. Macrì, A. Ridolfo, O. Di Stefano, A. F. Kockum, F. Nori, and S. Savasta, Phys. Rev. X **8**, 011031 (2018).

[28] J. R. Johansson, G. Johansson, C. M. Wilson, P. Delsing, and F. Nori, Phys. Rev. A **87**, 043804 (2013).

[29] Z. Tian, J. Jing, and A. Dragan, Phys. Rev. D **95**, 125003 (2017).

[30] N. S. S. de Buruaga and C. Sabín, Phys. Rev. A **95**, 022307 (2017).

[31] C. Sabín, I. Fuentes, and G. Johansson, Phys. Rev. A **92**, 012314 (2015).

[32] C. Sabín and G. Adesso, Phys. Rev. A **92**, 042107 (2015).

[33] X. Zhang, H. Liu, Z. Wang, and T. Zheng, Sci. Rep. **9**, 9552 (2019).

[34] Y. Long, X. Zhang, and T. Zheng, Quant. Info. Proc. **19**, 322 (2020).

[35] J. S. Bell, Phys. Phys. Fiz. **1**, 195 (1964).

[36] J. S. Bell, *Speakable and Unspeakable in Quantum Mechanics* (Cambridge University Press, Cambridge, England, 2004).

[37] A. Einstein, B. Podolsky, and N. Rosen, Phys. Rev. **47**, 777 (1935).

[38] D. Bohm, *Quantum Theory* (Prentice Hall, Englewood Cliffs, NJ, 1951).

[39] J. F. Clauser, M. A. Horne, A. Shimony, and R. A. Holt, Phys. Rev. Lett. **23**, 880 (1969).

[40] A. Aspect, P. Grangier, and G. Roger, Phys. Rev. Lett. **49**, 91 (1982).

[41] M. D. Reid and P. D. Drummond, Phys. Rev. Lett. **60**, 2731 (1988); M. D. Reid, Phys. Rev. A **40**, 913 (1989).

[42] D. F. Walls and G. J. Milburn, *Quantum Optics* (Springer-Verlag, Berlin, 1994).

[43] Z. Y. Ou, S. F. Pereira, H. J. Kimble, and K. C. Peng, Phys. Rev. Lett. **68**, 3663 (1992); Z. Y. Ou, S. F. Pereira, and H. J. Kimble, Appl. Phys. B **55**, 265 (1992).

[44] S. L. Braunstein, A. Mann, and M. Revzen, Phys. Rev. Lett. **68**, 3259 (1992).

[45] Z. B. Chen, J. W. Pan, G. Hou, and Y. D. Zhang, Phys. Rev. Lett. **88**, 040406 (2002).

[46] G. Gour, F. C. Khanna, A. Mann, and M. Revzen, Phys. Lett. A **324**, 415 (2004).

[47] M. Revzen, P. A. Mello, A. Mann, and L. M. Johansen, Phys. Rev. A **71**, 022103 (2005).

[48] M. M. Dorantes and J. L. Lucio M, J. Phys. A: Math. Theor. **42**, 285309 (2009).

[49] A. K. Ekert, Phys. Rev. Lett. **67**, 661 (1991).

[50] T. Jennewein, C. Simon, G. Weihs, H. Weinfurter, and A. Zeilinger, Phys. Rev. Lett. **84**, 4729 (2000).

[51] D. S. Naik, C. G. Peterson, A. G. White, A. J. Berglund, and P. G. Kwiat, Phys. Rev. Lett. **84**, 4733 (2000).

[52] W. Tittel, J. Brendel, H. Zbinden, and N. Gisin, Phys. Rev. Lett. **84**, 4737 (2000).

[53] U. Vazirani and T. Vidick, Phys. Rev. Lett. **113**, 140501 (2014).

[54] C. Miller and Y. Shi, J. ACM **63**, 1 (2016).

[55] R. Schwonnek *et al.*, Nat. Commun. **12**, 2880 (2021).

[56] S. Omkar, R. Srikanth, S. Banerjee, and A. K. Alok, Quantum Inf. Comput. **16**, 0757 (2016).

[57] D. Campo and R. Parentani, Phys. Rev. D **74**, 025001 (2006); J. Gallicchio, A. S. Friedman, and D. I. Kaiser, Phys. Rev. Lett. **112**, 110405 (2014).

[58] J. Martin and V. Vennin, Phys. Rev. D **96**, 063501 (2017).

[59] J. R. Johansson, N. Lambert, I. Mahboob, H. Yamaguchi, and F. Nori, Phys. Rev. B **90**, 174307 (2014).

[60] B. G. de Moraes, A. W. Cummings, and S. Roche, Phys. Rev. B **102**, 041403(R) (2020).

[61] R. Stassi, S. De Liberato, L. Garziano, B. Spagnolo, and S. Savasta, Phys. Rev. A **92**, 013830 (2015).

[62] A. Kalev, A. Mann, and M. Revzen, Found. Phys. **37**, 125 (2007).

[63] S. W. Ji, J. Lee, J. Park, and H. Nha, Sci. Rep. **6**, 29729 (2016).

[64] Y. Xiang, B. Xu, L. Mišta, Jr., T. Tufarelli, Q. He, and G. Adesso, Phys. Rev. A **96**, 042326 (2017).

[65] J. Singh and S. Bose, Phys. Rev. A **104**, 052605 (2021).

[66] M. Walschaers, V. Parigi, and N. Treps, PRX Quantum **1**, 020305 (2020).

[67] A. Ferraro and M. G. A. Paris, J. Opt. B: Quantum Semiclassical Opt. **7**, 174 (2005).

[68] S. Olivares and M. G. A. Paris, J. Opt. B: Quantum Semiclassical Opt. **7**, S392 (2005).

[69] P. C. Ugalde, *Experimental Prospects for Detecting the Quantum Nature of Spacetime* (UWSpace, Waterloo, Canada, 2017).

[70] A. Lambrecht, M. T. Jaekel, and S. Reynaud, Phys. Rev. Lett. **77**, 615 (1996).

[71] G. Adesso, S. Ragy, and A. R. Lee, Open Syst. Inf. Dyn. **21**, 1440001 (2014).

[72] D. T. Alves, C. Farina, and P. A. Maia Neto, J. Phys. A: Math. Gen. **36**, 11333 (2003).

[73] B. H. Schneider, A. Bengtsson, I. M. Svensson, T. Aref, G. Johansson, J. Bylander, and P. Delsing, Phys. Rev. Lett. **124**, 140503 (2020).

[74] M. Paternostro, H. Jeong, and T. C. Ralph, Phys. Rev. A **79**, 012101 (2009); C. Y. Park and H. Jeong, *ibid.* **91**, 042328 (2015).

[75] S. Schuermans, M. Simoen, M. Sandberg, P. Krantz, C. M. Wilson, and P. Delsing, IEEE Trans. Appl. Supercond. **21**, 448 (2011).

[76] H. M. Wiseman, S. J. Jones, and A. C. Doherty, Phys. Rev. Lett. **98**, 140402 (2007); S. J. Jones, H. M. Wiseman, and A. C. Doherty, Phys. Rev. A **76**, 052116 (2007).

[77] A. F. Abouraddy, T. Yarnall, B. E. A. Saleh, and M. C. Teich, Phys. Rev. A **75**, 052114 (2007).

[78] T. Yarnall, A. F. Abouraddy, B. E. A. Saleh, and M. C. Teich, Phys. Rev. Lett. **99**, 170408 (2007).

[79] G. Littich, Superconducting Mach-Zehnder interferometers for circuit quantum electrodynamics, Master's thesis, Laboratory for Solid State Physics, ETH Zürich, Switzerland, 2009.

[80] J.-A. Larsson, J. Phys. A: Math. Theor. **47**, 424003 (2014).

[81] M. Giustina *et al.*, Phys. Rev. Lett. **115**, 250401 (2015).